ORIGINAL ARTICLES

SEARCH FOR CORRELATIONS IN RAMAN, DIFFUSE REFLECTANCE, AND FLUORESCENCE SPECTROSCOPY DATA FROM INTRACRANIAL TUMORS

Ospanov A.[1], Romanishkin I.D.[2], Savelieva T.A.[1,2], Shugay S.V.[3], Kosyrkova A.V.[3], Pavlova G.V.[3,4], Pronin I.N.[3], Loschenov V.B.[1,2]
[1]National Research Nuclear University MEPhI (Moscow Engineering Physics Institute), Moscow, Russia
[2]Prokhorov General Physics Institute of Russian Academy of Sciences, Moscow, Russia
[3]N.N. Burdenko National Medical Research Center of Neurosurgery, Moscow, Russia
[4]Institute of Higher Nervous Activity and Neurophysiology of the Russian Academy of Sciences, Moscow, Russia

Abstract

The task of developing a decision support system in neurooncology based on optical-spectral analysis of intracranial tumor tissue is associated with several challenges inherent in working with biomedical data. These include the high dimensionality of the feature vector with a relatively small sample size, data gaps, and sample imbalances due to the varying frequencies of various diagnoses. Analysis of correlations between features of the tumors under study will allow both the restoration of data gaps and their augmentation (artificial expansion of the training dataset by creating modified versions of existing examples). This paper presents an analysis of the dependence of various optical-spectral characteristics on the tumor cell/tissue content in the sample and the cross-correlations between various features.

Key words: glial tumor, optical spectroscopy, Raman scattering, diffuse reflectance, fluorescence.

Contacts: Ospanov A., e-mail: ospanovanuar99@gmail.com

For citations: Ospanov A., Romanishkin I.D., Savelieva T.A., Shugay S.V., Kosyrkova A.V., Pavlova G.V., Pronin I.N., Loschenov V.B. Search for correlations in raman, diffuse reflectance, and fluorescence spectroscopy data from intracranial tumors, *Biomedical Photonics*, 2025, vol. 14, no. 4, pp. 22–33. doi:10.24931/2413–9432–2025–14-4-22-33

ПОИСК КОРРЕЛЯЦИЙ В ДАННЫХ СПЕКТРОСКОПИИ КОМБИНАЦИОННОГО РАССЕЯНИЯ, ДИФФУЗНОГО ОТРАЖЕНИЯ И ФЛУОРЕСЦЕНЦИИ ТКАНЕЙ ВНУТРИЧЕРЕПНЫХ ОПУХОЛЕЙ

А. Оспанов[1], И.Д. Романишкин[2], Т.А. Савельева[1,2], С.В. Шугай[3], А.В. Косырькова[3], Г.В. Павлова[3,4], И.Н. Пронин[3], В.Б. Лощенов[1,2]
[1]Национальный исследовательский ядерный университет «МИФИ» (Московский инженерно-физический институт), Москва, Россия
[2]Институт общей физики им. А.М. Прохорова Российской академии наук, Москва, Россия
[3]Национальный медицинский исследовательский центр нейрохирургии имени академика Н. Н. Бурденко, Москва, Россия
[4]Институт высшей нервной деятельности и нейрофизиологии Российской академии наук, Москва, Россия

Резюме

Задача построения системы поддержки принятия решений в нейроонкологии на основе оптико-спектрального анализа тканей внутричерепных опухолей сопряжена с некоторыми сложностями, свойственными работе с биомедицинскими данными. Среди них – высокая размерность вектора признаков при относительно малом объеме выборки, пропуски в данных, а также несбалансирован-

ность выборок из-за разной частоты встречаемости различных диагнозов. Анализ корреляций между признаками исследуемых опухолей позволит выполнять как восстановление пропусков в данных, так и их аугментацию (искусственное расширение обучающего набора данных путём создания модифицированных версий имеющихся примеров). В данной работе представлен анализ зависимости различных оптико-спектральных характеристик от содержания опухолевых клеток/ткани в образце и взаимных корреляций между различными признаками.

Ключевые слова: глиальная опухоль, оптическая спектроскопия, комбинационное рассеяние, диффузное отражение, флуоресценция.

Контакты: Оспанов А., e-mail: ospanovanuar99@gmail.com

Для цитирования: Оспанов А., Романишкин И.Д., Савельева Т.А., Шугай С.В., Косырькова А.В., Павлова Г.В., Пронин И.Н., Лощенов В.Б. Поиск корреляций в данных спектроскопии комбинационного рассеяния, диффузного отражения и флуоресценции тканей внутричерепных опухолей // Biomedical Photonics. – 2025. – Т. 14, № 4. – С. 22–33. doi: 10.24931/2413-9432-2025-14-4-22-33

Introduction

Determining the boundaries of intracranial tumors is a central problem in neuro-oncology today. The magnetic resonance imaging (MRI) is limited as intraoperative tools, and ultrasound does not provide information on tumor metabolic parameters. Therefore, intraoperative optical neuroimaging [1-3] and laser spectroscopy [4,5] have become increasingly important.

Fluorescence spectroscopy techniques are highly dependent on the photosensitizer concentration in the tissue being examined. If the photosensitizer has not accumulated in sufficient quantities in the tissue, fluorescence analysis may be uninformative. Raman spectroscopy (RS) can be a useful complement to fluorescence diagnostic methods. RS does not require photosensitizer accumulation. However, due to the specific features of Raman spectra, namely, the large number of significant peaks and lower signal intensity compared to fluorescence, Raman spectra require more complex signal preprocessing and statistical analysis of the results [6].

Machine learning methods can be used to preprocess and analyze measurement results, particularly Raman spectra. A brief overview of simple machine learning methods for preprocessing data obtained from IR and Raman spectra is provided in [7]. Dimensionality reduction algorithms are one such method. It is the process of reducing the size of a feature vector. A set of features can be a dataset with hundreds of columns or an array of points that form a large sphere in three-dimensional space. As the number of features increases, the number of dimensions also increases proportionally. The more features describe one object, the more objects in the sample we need to ensure that all combinations of feature values are well represented.

Machine learning algorithms can also be used for data analysis, which can be divided into supervised and unsupervised learning. Unsupervised learning works on unlabeled data, without human intervention. An example of an unsupervised learning approach is data clustering. Supervised learning is a method in which a model learns to solve problems based on examples with known answers.

In [6], dimensionality reduction and clustering algorithms were considered for data obtained using fluorescence, diffuse reflectance, and Raman scattering from intracranial tumor biopsies. It shows that an algorithm without training on unlabeled data can distinguish meningeal and glial tumors with good accuracy. The use of more advanced algorithms will make it possible to distinguish between the types and stages of tumors.

Machine learning methods for spectroscopy have become widespread. In [8], neural network algorithms were applied to data obtained using surface-enhanced Raman scattering for pathogen recognition. An excellent example of data classification using machine learning is the work [9], where for classification random forest algorithms and the gradient boosting tree method were used. The objects of classification were Raman spectroscopy data obtained from fresh specimens of glial tumors, which overlaps with the objects studied in our article. Analysis of the application of machine learning methods to spectrally resolved data in neurooncology [10,11] shows that they can be successfully applied to the classification of intracranial tumors, which is what we aim to achieve.

However, we would like to move from classical machine learning methods to neural network-based ones, but the number of experimental specimens we've analyzed to date is insufficient. Samples for different diagnoses vary significantly in the number of specimens they contain. To overcome these limitations in the application of neural network algorithms, we propose expanding groups with small numbers of objects with artificial data – in other words, data augmentation. To successfully implement augmentation, as well as to study the relationships between measured data, we decided to conduct a correlation analysis of the available data, which is the focus of this article.

Interesting application of correlation analysis is presented in the work [12], in which the authors examine brain gliomas and calculate correlation coefficients to validate a previously studied machine learning algorithm that sequentially generates a cellularity prediction map.

Materials and methods

Biological specimens

In total (after removing outliers), more than 250 fresh tissue samples from intracranial brain tumors (hereinafter referred to as biopsies) were examined. Of these, the following were diagnosed:

- Meningioma – 66 specimens (38 – grade I, 21 – grade II, 7 – grade III);
- Glioblastoma – 112 specimens;
- Oligodendrogliomas – 32 specimens (4 with unknown grade; 8 – grade II; 20 – grade III);
- Astrocytomas – 41 specimens (12 with unknown grade; 1 – grade I; 2 – grade II; 26 – grade III).

Experimental stand for spectral analysis

A He-Ne laser (632.8 nm wavelength) and a diode laser (405 nm wavelength) were used to excite the fluorescence signal in biological samples. LESA-01-BIOSPEC spectrometers with optical edge filters attenuating the excitation light (632.8 and 405 nm) at the spectrometer input to the fluorescence signal level were used to record the fluorescence spectra. An optical fiber was used to deliver the laser signal. A halogen lamp and a LESA-01-BIOSPEC spectrometer were used as a white light source to record diffuse reflectance. Raman spectra were measured using a Raman-HR-TEC-785 spectrometer (StellarNet, USA; spectral range 200–2750 cm^{-1}, resolution 4 cm^{-1}), a Ramulaser-785 laser source (StellarNet, USA; 785 nm), and a fiber-optic confocal probe for delivering laser radiation and a Raman signal. The laser peak width is 0.2 nm; power up to 500 mW. Spectral measurements were performed in a darkened room.

Sample collection protocol

The sampling protocol was presented in the following steps:

1. Transfer of brain tumor fragments (biopsy specimens) removed by the surgeon during surgery (cleaned of extrinsic material and placed in saline) to the cryopreservation laboratory for preliminary tissue characterization prior to freezing. Prior to spectroscopic measurements, the specimen is kept at 4°C (specimens were measured no later than 4 hours later).
2. Selection of one to three fragments of 2-5 mm in diameter from the available tumor material. If a fragment is larger than the dimensions described above, it is divided into parts, as larger fragments may have inhomogeneous structure.
3. Darkening the room and measuring the background signal (baseline) of the Raman spectrometer for subsequent software exclusion.
4. Calibration of fluorescence spectrometers (LESA with filters at 405 and 632.8 nm) by wavelengths using 3 lasers: 405, 532, 632.8 nm.
5. The fluorescence spectra of protoporphyrin IX (Pp IX) and the autofluorescence spectra are measured using the LESA-01-BIOSPEC spectrometer (Biospec, Russia) using a common algorithm: the appropriate laser (632.8 nm or 405 nm) is turned on, the distal end of the light guide is brought into soft contact with the sample, and several spectra from different points on each sample are recorded (approximately six measurements). The exposure time is 100 ms.
6. Measurement of diffuse reflectance spectra is performed using a LESA-01-BIOSPEC spectrometer (with a halogen lamp as a white light source) and includes measurement of the baseline, the reference signal in the reflectance mode from a white sample (barium sulfate), measurement of spectra from an object in the diffuse reflectance mode (with the distal end of the light guide in soft contact with the sample, several (about 6) measurements are made for each sample).
7. Measurements of Raman spectra are performed with an exposure of 30 s, 10 measurements from each sample (the power of the 785 nm laser is 150 mW).
8. After measurements, the sample is placed in formalin and given to a morphologist for histological examination.

The process of sampling and recording optical spectra was carried out in the Department of Cryopreservation and Molecular Genetic Analysis of the N.N. Burdenko National Medical Research Center of Neurosurgery.

Spectrum processing

Uno software (Biospec, Russia) was used to process fluorescence and diffuse reflectance spectra. Processing of Raman spectra and subsequent analysis of both fluorescence, diffuse reflectance, and Raman spectra were performed using specialized software developed in Python within the Jupiter Notebook environment.

Components of feature vector were extracted from fluorescence, diffuse reflectance, and Raman spectra. A matrix was formed from the feature vectors of the specimens, which is used for data analysis (in this case, for correlation analysis).

From fluorescence excited by a 632.8 nm laser, backscatter (diffuse reflectance) of laser radiation and Pp IX fluorescence were extracted as features.

From fluorescence excited by a 405 nm laser, diffuse reflectance (diffuse reflectance) of laser radiation and the fluorescence of FAD and porphyrins were extracted. The contribution of diffuse reflectance of broadband radiation to the feature vector is represented by hemoglobin absorption, its oxygen saturation, and the scattering coefficient.

The largest number of feature vector components were taken from the Raman spectra. When choosing which data from the Raman spectra to take as features, the authors relied on the work [7] and also searched for biochemical components that showed the presence of statistically significant differences between the groups [13]. The following biochemical components were taken from the Raman spectra as features: cholesterol; phospholipid; lipids; carotenoids; heme/hemoglobin; oxygenated heme/hemoglobin; proteins; phenylalanine.

Explanation of legenda on Figures for feature vector components are given in Table.

A more detailed description of the methodology is given in our previous works [14,15].

Correlation analysis

Correlation analysis is a statistical method for determining the relationship between two sets of variables (in this case, features in feature vector). The key parameter of this method is the correlation coefficient, which indicates the type of relationship. The correlation coefficient can take values from –1 to 1. Values close to –1 indicate an inverse relationship between the variables, values close to 1 indicate a direct relationship, and values close to 0 indicate no relationship. A very important parameter related to the correlation coefficient is its statistical significance. It allows one to assess the validity of the conclusion

Таблица
Список основных оптико-спектральных параметров и их условных обозначений
Table
List of main optical-spectral parameters and their symbols

Условное обозначение Legend	Оптико-спектральные параметры Optical-spectral parameters
backscatter_633	Обратное рассеяние от 632,8 нм лазера Diffuse reflectance of 632.8 nm laser light
fluo_633	Флуоресценция от 632,8 нм лазера (ассоциированная с протопорфирином IX) Fluorescence excited with 633 nm laser light (associated with Pp IX)
backsca_405	Обратное рассеяние от 405 нм лазера Diffuse reflectance of 405 nm laser light
fluo_405_fad	Флуоресценция флавинов, преимущественно ФАД (флавинадениндинуклеотида) от 405 нм лазера Fluorescence excited with 405 nm laser light (associated with flavins, mainly FAD)
fluo_405_porph	Флуоресценция от 405 нм лазера (ассоциированная с протопорфирином IX) Fluorescence excited with 405 nm laser light (associated with Pp IX)
hemoglobin	Поглощение гемоглобина, определяемый по спектру диффузного отражения от белого источника Hemoglobin calculated from diffuse reflectance spectra
scattering	Коэффициент рассеяния, определяемый по спектру диффузного отражения от белого источника Scattering coefficient calculated from diffuse reflectance spectra
r_cholesterol	Комбинационное рассеяние от холестеринов Raman scattering from cholesterol
r_phospholipid	Комбинационное рассеяние от фосфолипидов Raman scattering from phospholipid
r_lipid	Комбинационное рассеяние от липидов Raman scattering from lipids
r_carothenoid	Комбинационное рассеяние от каротиноидов Raman scattering from carotenoids
r_heme	Комбинационное рассеяние от гема Raman scattering from heme
r_oxy_heme	Комбинационное рассеяние оксигинированного гема Raman scattering of oxygenated heme
r_protein	Комбинационное рассеяние от белков Raman scattering from proteins
r_phenylalanine	Комбинационное рассеяние от фенилаланина Raman scattering from phenylalanine

regarding the presence of a correlation relationship obtained using the correlation coefficient. The lower the significance value, the stronger the correlation relationship described by the correlation coefficient.

In this study, the Spearman rank correlation coefficient was used. This coefficient was chosen because the authors currently have a small amount of data. The Spearman rank correlation coefficient is calculated using formula (1):

$$\rho = \frac{\sum_{i=1}^{n}(x_i - \bar{x})(y_i - \bar{y})}{\sqrt{\sum_{i=1}^{n}(x_i - \bar{x})^2 (y_i - \bar{y})^2}}, \quad (1)$$

where n – number of observations; $\bar{x}$ и $\bar{y}$ – average values.

The statistical significance of the correlation coefficient (1) is determined using the Student's t-test according to the formula (2):

$$t = \frac{\rho\sqrt{(n-2)}}{\sqrt{(1-\rho^2)}}. \quad (2)$$

Calculations of correlation coefficients and their statistical significance were performed using Python programming language and the Jupiter Notebook programming environment. Correlation coefficients were calculated for all feature vectors with each other, as well as correlations between feature vectors and the tumor percentage (percentage of tumor cells) of the biopsy specimen. Fig. 1 shows a generalized diagram of the analysis of biomaterial and its spectral characteristics for the purpose of automating classification, which shows the place that the topic of this article has in this concept.

Results and discussion

Correlation of features with the percentage of tumor in the sample

In order to analyze the physiological correlates of the spectral characteristics of tumors, we carried out a study of the relationship between all known characteristics of the samples, such as features obtained from the pathological report (tumor type glioma/meningioma/oligodenroglioma, tumor grade, percentage of tumor in the sample) and from spectral analysis (presence of various biochemical components and optical characteristics).

The results of the pathomorphological examination allow us to analyze the correlations between the measured optical-spectral characteristics and the content of tumor or necrotic cells/tissue in the sample. Since classification results depend significantly on the percentage of tumor in the sample at which we classify it as a tumor, and the percentage of necrotic tissue at which we classify it as necrosis, we conducted studies of the threshold values for various characteristics.

Fig. 2 shows the summary results of the detected dependencies, which allowed us to identify so-called "healthy tissue correlates," that is, spectral characteristics that are higher in normal tissue, and "tumor tissue correlates," that is, parameters that are higher in tumor and necrotic tissue. A non-monotonous relationship with the percentage of tumor in the sample was also found for lipids and phospholipids, which was the subject of a separate study, described below.

We included carotenoids (r_carothenoid) and oxygenated hemoglobin (r_oxy_heme) among the healthy tissue correlates (Fig. 3a). The carotenoid

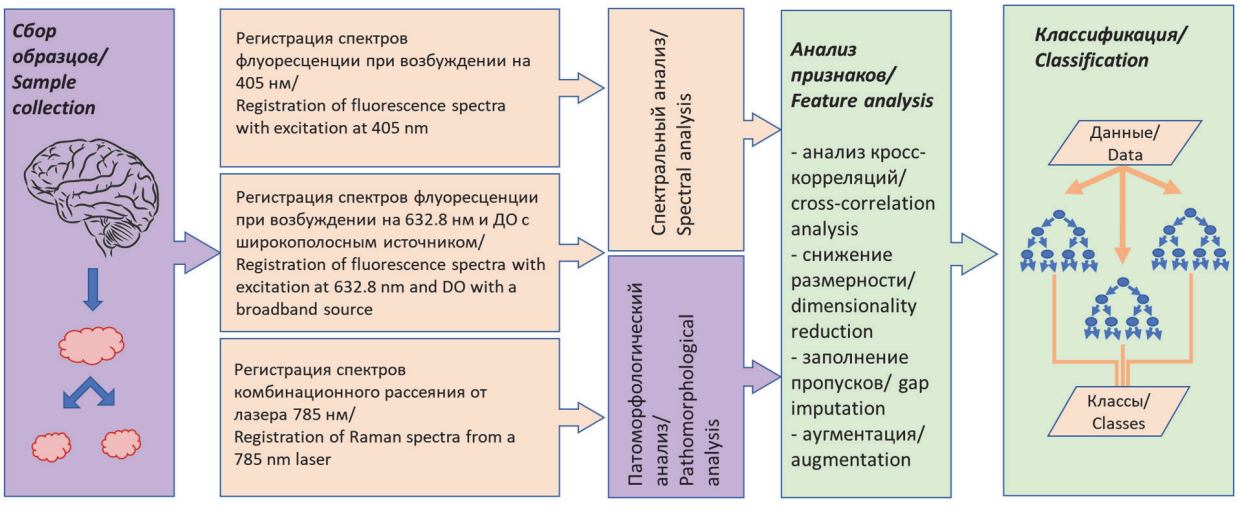

Рис. 1. Схема анализа образцов и данных при построении модели классификации внутричерепных опухолей по данным оптической спектроскопии.
Fig. 1. Scheme of sample and data analysis when constructing a model for classifying intracranial tumors based on optical spectroscopy data.

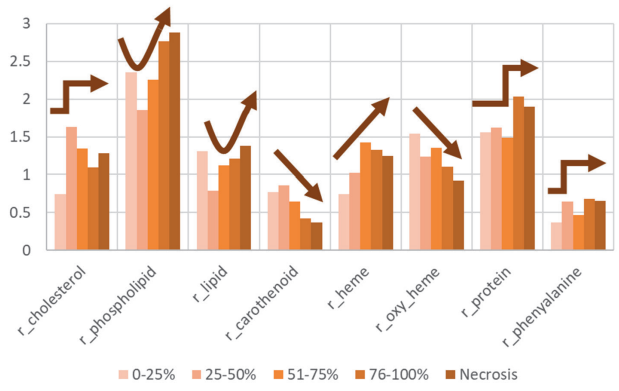

Рис. 2. Зависимость оптико-спектральных характеристик КР от содержания опухолевых тканей в образце.
Fig. 2. Dependence of optical-spectral characteristics from Raman spectra on the content of tumor tissue in the sample.

and oxygenated hemoglobin content in the samples inversely correlated with the percentage of tumor tissue in the sample, since carotenoids are a component of the antioxidant defense system in normal tissues, while tumor tissues are hypoxic. Previous studies have shown that carotenoid concentrations in plasma are inversely proportional to cancer risk in epidemiological and experimental studies. Carotenoids are specifically distributed in different lymphocyte subtypes. Zhou et al. [16] observed a clear decrease in the intensity of the 1157 and 1521 cm^{-1} peaks with an increase in the degree of malignancy of gliomas. Hypoxia also correlates with the degree of tumor malignancy [17].

When it comes to tumor tissue correlates, hemoglobin (r_heme) is, of course, the primary one. Blood volume correlates with the level of vascularization and the degree of malignancy in gliomas [18,19], and the density of microvessels in gliomas can be an independent prognostic factor [20, 21]. This is precisely the nature of the dependence on the tumorigenicity of the sample that we observe with a significance level of 1% for heme, determined using Raman spectroscopy (Fig. 3b).

In Fig. 3, we also see that cholesterol (r_cholesterol) increased with increasing tumor tissue content in the sample. However, the data spread was so wide that the significance level of differences between groups for this parameter was 18%. Tumor tissues were also characterized by higher protein content (r_protein). It should be noted that forming these groups required partitioning with different tumorigenicity thresholds:

- Cholesterol levels in specimens with 26% or more tumor tissues (including necrosis) are significantly higher than in specimens with 0–25% tumor tissues;

- Heme levels in specimens with 51% or more tumor tissues (including necrosis) are significantly higher than in specimens with 0–50% tumor tissues;
- Protein levels in specimens with 76% or more tumor tissues (including necrosis) are significantly higher than in specimens with 0–75% tumor tissues.

This suggests the need for a finer division of specimens into classes for some characteristics, as well as a continuous change in these characteristics in general.

Correlations between spectral features

Correlation coefficients for features were examined to identify relationships between them. For each pair of features, Spearman's rank correlation coefficients and

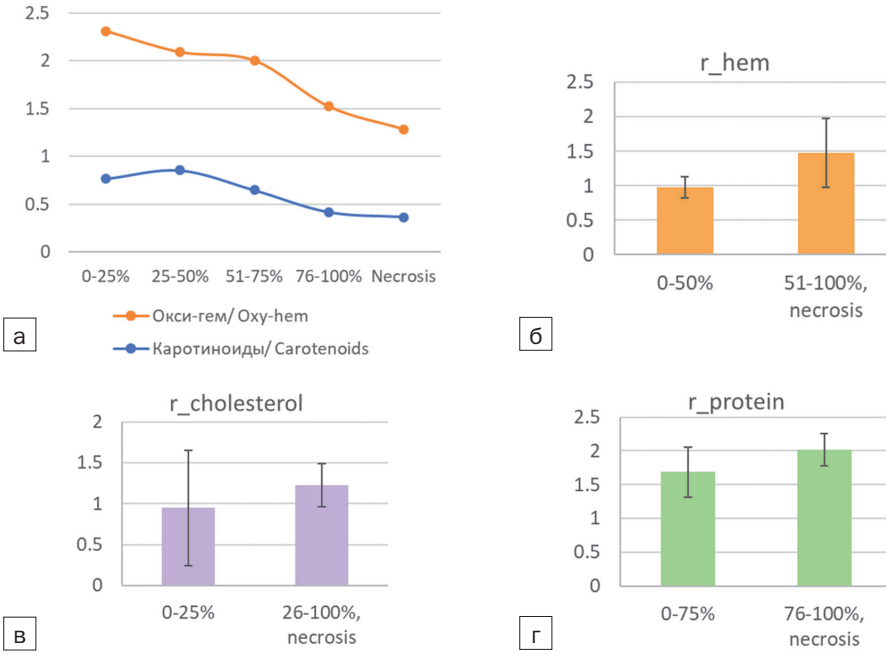

Рис. 3. Корреляты здоровых и опухолевых тканей (включая ткани с некротическими включениями).
Fig. 3. Correlates of healthy and tumor tissues (including tissues with necrosis).

statistical significance for each correlation coefficient were calculated. As a criterion of interest, as well as a certain statistical significance of the correlation between features, we took the threshold value of the rank correlation coefficient by modulus of 0.7 or higher, and the value of statistical significance of 0.05 or less. Feature vectors satisfying the above condition are called feature vectors satisfying the criterion of interest. Fig. 5-9 show graphs of the dependencies of feature vectors satisfying the criterion of interest with correlation coefficients and with the statistical significance of the correlation coefficients. A comparison was also made of the spectral features determined from the diffuse reflectance and Raman spectra, which showed a non-monotonic dependence on the content of tumor tissue in the sample.

Correlation of diffuse reflectance and Raman scattering features

In our previous study [15], we compared light scattering in tumors recorded intraoperatively and during studies in biobank. Similar patterns were demonstrated, with a minimum for the perifocal zone in intraoperative studies, which we compared with the light scattering minimum for samples containing 26–50% tumor tissue during data analysis in biobank. We explained this nontrivial behavior of the parameter by the gradual degradation of normal white matter during tumor development, which competes in its effect with the growth of tumor cell content. Light scattering in tissues occurs due to fluctuations in the refractive index of the medium. The main source of these fluctuations are lipids in cell membranes, which is especially relevant for the white matter of the brain, which comprises 50% of the myelin sheaths of nerve tracts. In this study, we compared these diffuse reflectance data with the results of lipid and phospholipid analysis, which, as shown in Fig. 2 and 4, also demonstrate a local minimum for the same samples. A study of the lipid and phospholipid content in tumor samples using Raman spectra revealed the same "saddle-shaped" dependence on the tumor percentage of the samples (Fig. 4).

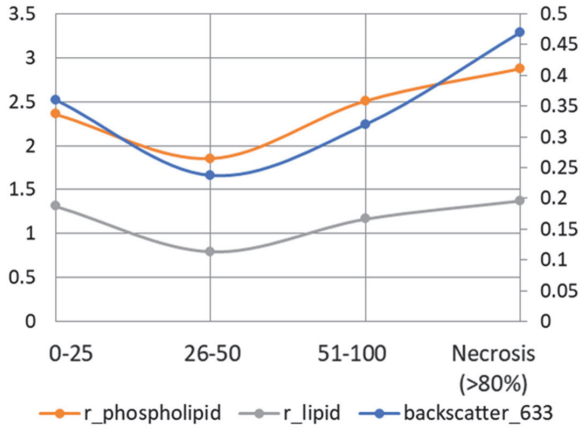

Рис. 4. Корреляция сигнала диффузного отражения и содержания липидов и фосфолипидов.
Fig. 4. Correlation of diffuse reflectance signal and content of lipid and phospholipid.

Meningiomas

66 samples diagnosed with meningioma were examined and analyzed in total. Of these, 38 were grade I meningiomas, 21 were grade II meningiomas, and 7 were grade III meningiomas.

Fig. 5 shows two dependences of features that meet the criteria of interest for grade I meningioma. A positive correlation is observed between the fluorescence of Pp IX (fluo_405_porph) and FAD (fluo_405_fad) upon excitation by laser radiation with a wavelength of 405 nm (Fig. 5a). In Fig. 5b, a direct correlation is observed between the Raman scattering of proteins (r_protein) and phospholipids (r_phospholipid). According to work [22], phospholipids in Raman spectra are most strongly manifested in the white matter of the brain, stronger in normal tissue, weaker in a tumor, but stronger in necrotic tissue than in a tumor. If we look at Fig. 2 in this article, we will see just such a non-monotonic dependence of the expression of the presence of phospholipids on the percentage of tumor in the sample with a local minimum falling approximately in the range of 25–50%. Moreover, the protein presence index demonstrates a fairly significant increase when moving to samples with a tumor prevalence of more than 50%. According to surface-enhanced Raman spectroscopy data [23], the presence of proteins is higher, including in glioblastomas.

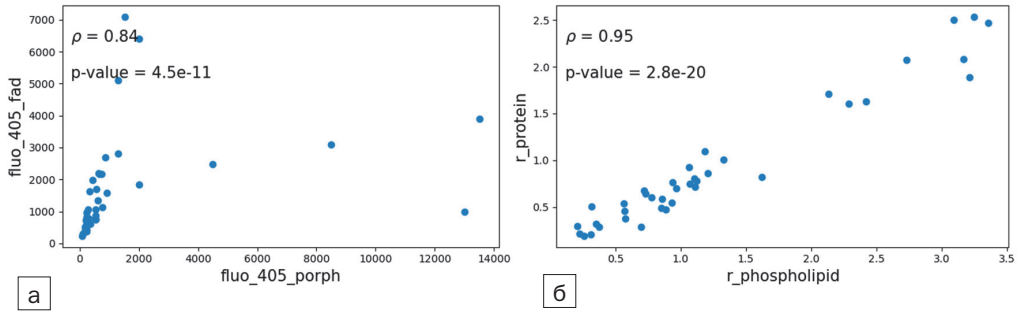

Рис. 5. Графики зависимости компонент вектора признаков, удовлетворяющих критерию интереса для менингиом I степени.
Fig. 5. Graphs of the dependence of the components of the feature vector satisfying the criterion of interest for grade I meningiomas.

Fig. 6a shows a correlation between PP IX (fluo_405_porph) and FAD (fluo_405_fad) similar to Fig. 5a. Work [24] showed that free FAD is present to a greater extent in grade II meningioma than protein-bound FAD, and it is more concentrated in grade II meningioma than grade I, while control samples show a higher frequency of protein-bound FAD and a decrease in the concentration of free FAD. In [25], fluorescence analysis was performed using a modified surgical microscope. Data were obtained on flavin fluorescence in the 500–580 nm range and the integrated fluorescence spectrum in the 430–740 nm range in freshly removed samples of various brain tumors: low- and high-grade gliomas, meningiomas, and metastases. It was shown that the fluorescence of protein-bound flavin mononucleotide (FMN) in brain tumors increased with a shift in metabolism toward a more glycolytic mode. These metrics were characteristic of various tumors and demonstrated the potential for their use in machine learning-based classification of brain tumors. The increased accumulation of Pp IX within tumor cells is likely due to the difference in cell proliferation between tumor and healthy tissues. In particular, porphobilinogen deaminase activity increases during replication [26]. Another enzyme with altered activity in tumor cells is ferrochelatase, whose reduced expression has been demonstrated in many tissues and tumors, including glioblastoma [27, 28]. This condition promotes a longer presence of Pp IX inside the cells, which may also be associated with the intensity of their fluorescence [29, 30]. Thus, the fluorescence correlation in this case appears to be consistent, and we can extend this pattern to all types of tumors analyzed in this work.

Glial tumors

A total of 185 glial tumors were examined. Of these: glioblastomas – 112; oligodendrogliomas – 28 (grade II – 8; grade III v 20; unknown grade – 4); astrocytomas – 41 (grade I – 1; grade II – 2; grade III – 26, unknown grade – 12).

Fig. 7 shows the cross-correlations of parameters for oligodendrogliomas, demonstrating the maximum relationship between the features. Among these, maximum values of the correlation coefficient are between the fluorescence of Pp IX (fluo_405_porph) and FAD (fluo_405_fad) upon excitation with a 405 nm laser (ρ = 0.97) and between the indices of protein (r_protein) and phospholipid (r_phospholipid) presence, calculated from Raman spectra (ρ = 0.98).

General considerations regarding these relationships were discussed above in the section on meningiomas. The high correlation between phospholipids (r_phospholipid) and heme (r_heme) appears quite

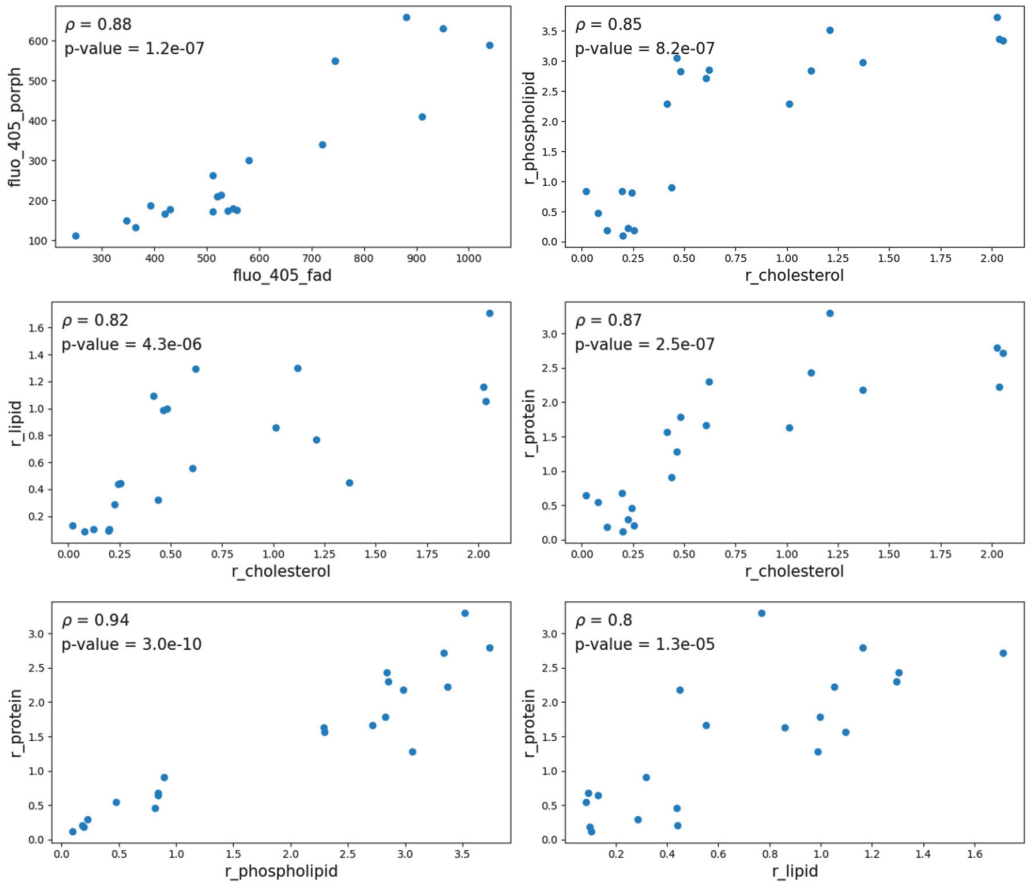

Рис. 6. Графики зависимости векторов признаков, удовлетворяющие критерию интереса для менингиомы II степени.
Fig. 6. Graphs of the dependence of feature vectors satisfying the criterion of interest for grade II meningioma.

expected, as we already identified heme as a correlate of tumor tissue, and the increasing expression of phospholipid spectral lines with increasing tumor tissue content of the samples, starting from 50%, also allows us to consider them in this way. However, the non-monotonic dependence of the phospholipid signal on the tumor tissue content means that higher values can also be observed at lower, "healthy," heme concentrations, which is reflected in the corresponding diagram in Fig. 7 by the wide scatter.

Moreover, the high correlation of phospholipids with oxygenated heme appears secondary to the previous case, as it is due to the generally higher hemoglobin content in tumor tissues. Furthermore, we see very high variability in oxygenated hemoglobin with high phospholipid content for two reasons: it could be healthy tissue, which has a higher phospholipid content and a higher hemoglobin saturation level; or it could be a tumor, which is more hypoxic, but has a higher overall heme content, meaning a higher absolute value of oxygenated hemoglobin. The correlation of such features as heme and proteins, as well as lipids and phospholipids, does not require additional explanation. Phenylalanine, despite the fact that it shows high values of correlation coefficients with many parameters, demonstrates a tendency towards clustering of values. According to [22, 23], the phenylalanine Raman signal is higher in glioblastoma, astrocytoma, and necrosis than in normal tumors, stronger in necrosis than in tumors, elevated in high-grade tumors, and slightly elevated after radiation therapy. Fig. 2 in our work shows that its relationship with tumorigenesis is ambiguous. Further research will likely be required to evaluate its role.

For anaplastic astrocytoma, we can see a high correlation, already demonstrated previously for

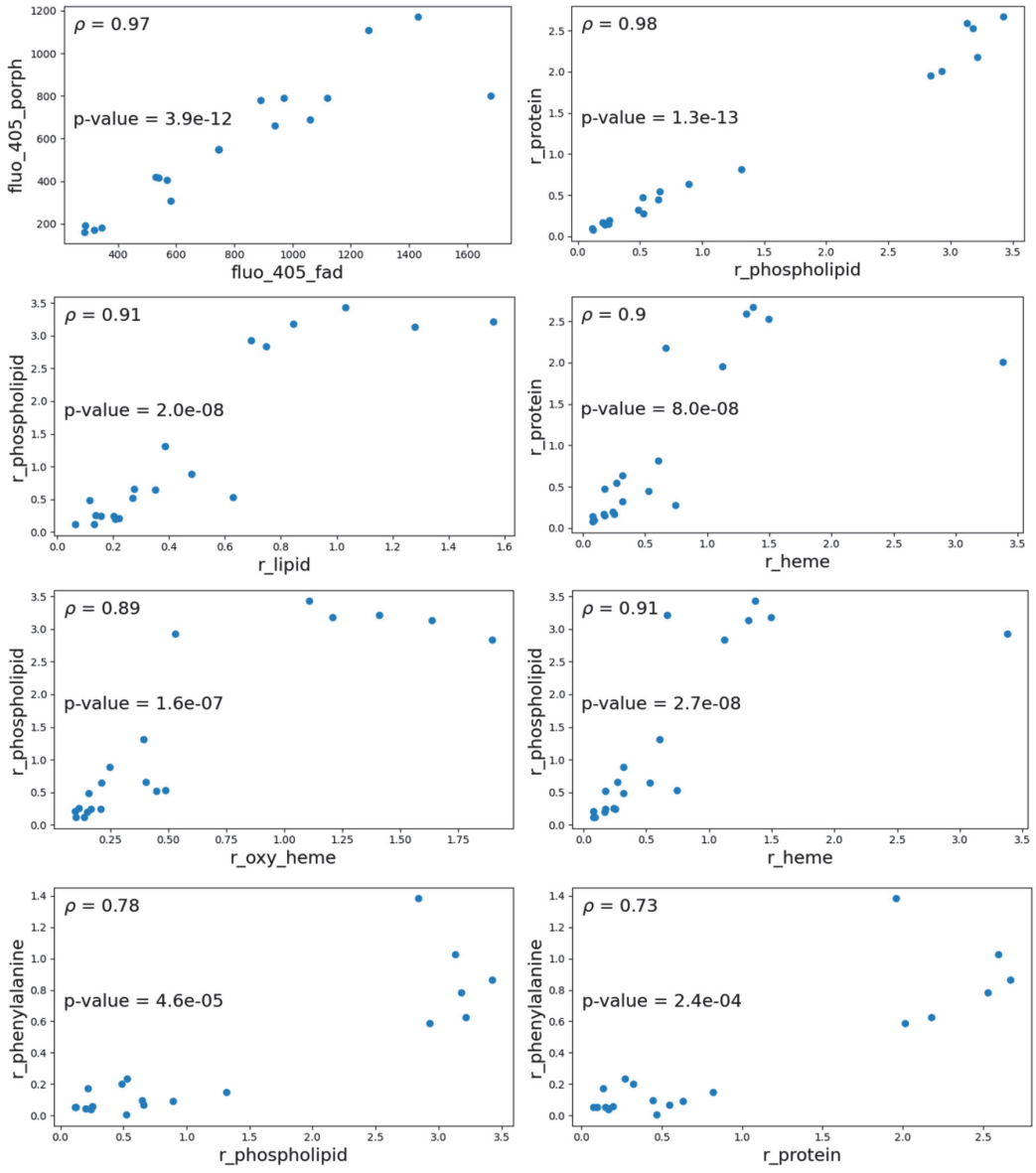

Рис. 7. Графики взаимных корреляций отдельных компонент вектора признаков, удовлетворяющие критерию интереса для олигодендроглиомы III степени.
Fig. 7. Graphs of mutual correlations of individual components of the feature vector satisfying the criterion of interest for oligodendroglioma grade III.

other tumors and explained above (Fig. 8). Analysis of glioblastomas (Fig. 9) reveals a predictably high data variability across all parameters, as this is a highly heterogeneous tumor. However, we can identify fairly strong correlations between proteins and phospholipids, as discussed above, proteins and heme, both total and oxygenated (apparently due to heme being a prosthetic group of the protein molecule), lipids and phospholipids, and between heme and phenylalanine.

Conclusions

An analysis of correlations between the features of the intracranial tumors studied, calculated based on fluorescence, diffuse reflectance, and spontaneous Raman spectra, and the tumor tissue content in the specimens, allowed us to identify spectral correlates of healthy tissues, such as carotenoids and oxygenated heme, as well as tumor tissue correlates, such as heme, cholesterol, and proteins. An analysis of cross-correlations between spectral features revealed a relationship between the autofluorescence of FAD and Pp IX, as well as phospholipids and proteins. This analysis, combined with data of tumor tissue content, explains the greater scatter of results with higher phospholipid content. Other features showed significant correlations, usually due to a common chemical nature.

This work was supported by the Ministry of Science and Higher Education of the Russian Federation (the Federal Scientific-technical program for genetic technologies development for 2019–2030), agreement №075-15-2025-559

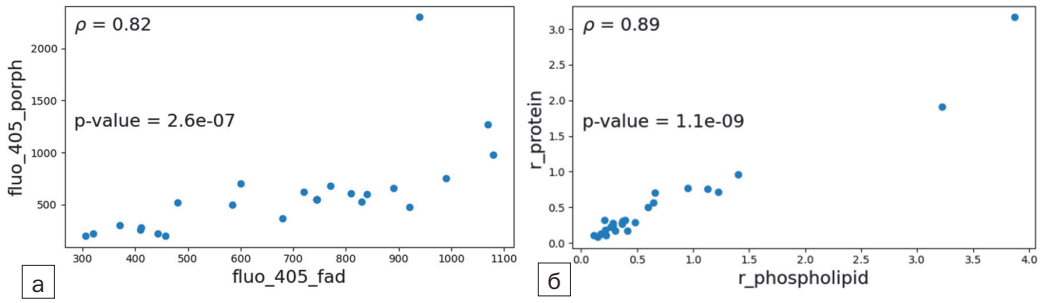

Рис. 8. Графики зависимости признаков, удовлетворяющие критерию интереса для астроцитомы III степени.
Fig. 8. Graphs of the dependence of features satisfying the criterion of interest for astrocytoma grade III.

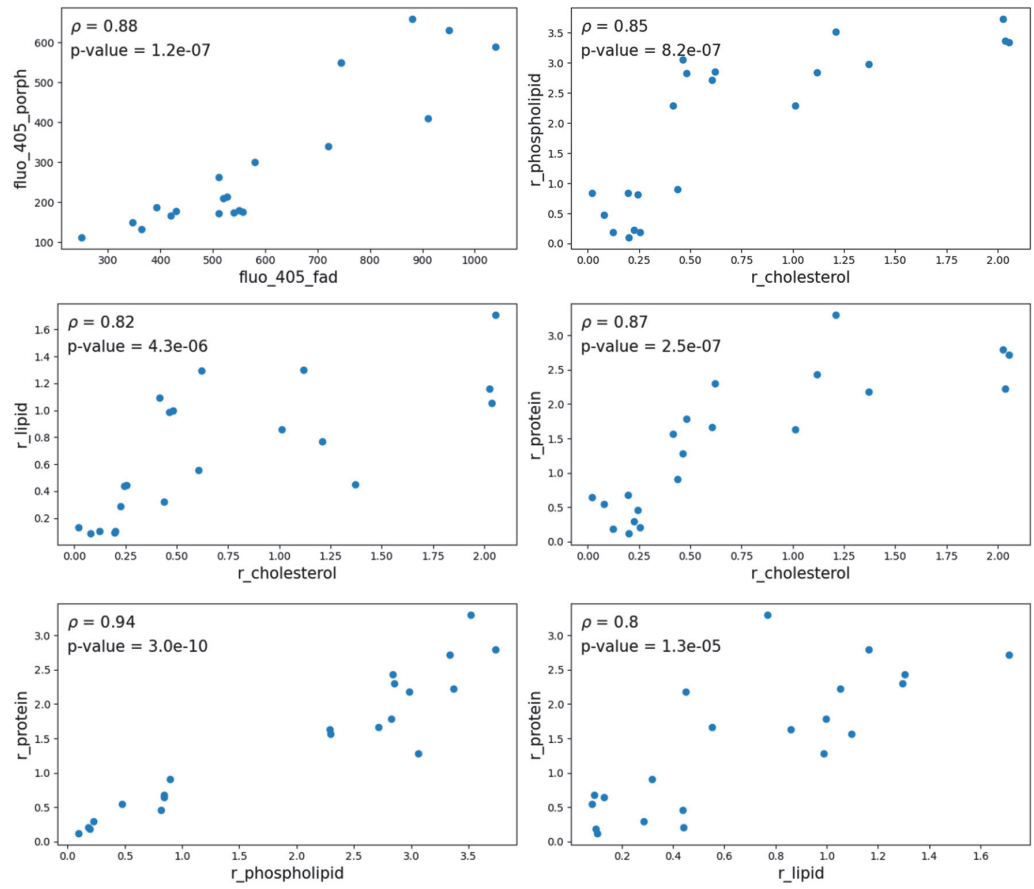

Рис. 9. Графики зависимости векторов признаков, удовлетворяющие критерию интереса для глиобластом.
Fig. 9. Graphs of the dependence of feature vectors satisfying the criterion of interest for glioblastomas

REFERENCES

1. Bailey D., Zacharia B.E. Intraoperative imaging techniques to improve tumor detection in the surgical management of gliomas // Adv. Cancer Res. – 2025. – vol. 166, pp. 103–135. doi: 10.1016/bs.acr.2025.05.001
2. Rynda A.Yu., Olyushin V.E., Rostovtsev D.M., et al. Results of microsurgical resection of glioblastomas under endoscopic and fluorescent control // Biomedical Photonics. – 2024. – vol. 13. – pp. 20-30. doi: 10.24931/2413-9432-2024-13-3-20-30
3. Goryaynov S.A., Okhlopkov V.A., Golbin D.A., et al. Fluorescence Diagnosis in Neurooncology: Retrospective Analysis of 653 Cases // Front. Oncol. – 2019. – vol. 9. – pp. 830. doi: 10.3389/fonc.2019.00830
4. Potapov AA, Goriaïnov SA, Loshchenov VB, et al. Intraoperative combined spectroscopy (optical biopsy) of cerebral gliomas. Burdenko's Journal of Neurosurgery. – 2013. – vol. 77. – pp. 3-10.
5. Stupak E.V., Glotov V.M., Askandaryan A.S. et al. Raman Spectroscopy in the Diagnosis of Brain Gliomas: A Literature Review // Cureus. – 2025. – vol. 17 – pp. – e79165. doi: 10.7759/cureus.79165.
6. Ospanov A., Romanishkin I., Savelieva T. et al. Optical Differentiation of Brain Tumors Based on Raman Spectroscopy and Cluster Analysis Methods // Int. J. Mol. Sci. – 2023. – vol. 24. – pp. 14432. doi: 10.3390/ijms241914432
7. Gautam, R., Vanga, S., Ariese, F. et al. Review of multidimensional data processing approaches for Raman and infrared spectroscopy // EPJ Techn Instrum. – 2015. – vol. 2. doi: 10.1140/epjti/s40485-015-0018-6
8. Lee J, Huh J. Pathogen Recognition via Surface-Enhanced Raman Scattering: Self-Supervised Learning and Transfer Learning approaches // ChemRxiv. – 2025. – doi:10.26434/chemrxiv-2025-cmr8g.
9. Riva M., Sciortino T., Secoli R. et al. Glioma biopsies Classification Using Raman Spectroscopy and Machine Learning Models on Fresh Tissue Samples // Cancers (Basel). – 2021. – vol. 13. – pp. 1073. doi: 10.3390/cancers13051073.
10. Savelieva T., Romanishkin I., Ospanov A. et al. Machine Learning and Artificial Intelligence Systems Based on the Optical Spectral Analysis in Neuro-Oncology // Photonics. – 2025. – vol. 12. – pp. 37. doi: 10.3390/photonics12010037.
11. Savelieva T.A., Romanishkin I.D., Ospanov A. et al. Machine learning methods for spectrally-resolved imaging analysis in neuro-oncology. Biomedical Photonics // 2024. – vol. 13. – pp. 40-54. doi: 10.24931/2413-9432-2024-13-4-40-54.
12. Nocera G., Sanvito F., Yao J. et al. Independent histological validation of MR-derived radio-pathomic maps of tumor cell density using image-guided biopsies in human brain tumors // J Neurooncol. – 2025. doi: 10.1007/s11060-025-05105-x.
13. Romanishkin I., Savelieva T., Kosyrkova A. et al. Differentiation of glioblastoma tissues using spontaneous Raman scattering with dimensionality reduction and data classification // Front Oncol. – 2022. – vol. 12. – pp. 944210. doi: 10.3389/fonc.2022.944210.
14. Romanishkin I.D., Savelieva T.A., Ospanov A. et al. Classification of intracranial tumors based on optical-spectral analysis // Biomedical Photonics. – 2023. – vol. 12. – pp. 4-10. doi: 10.24931/2413-9432-2023-12-3-4-10.
15. Romanishkin I.D., Savelieva T.A., Ospanov A. et al. Comparison of optical-spectral characteristics of glioblastoma at intraoperative diagnosis and ex vivo optical biopsy // Biomedical Photonics. – 2024. – vol. 13. – pp. 4-12. doi: 10.24931/2413-9432-2024-13-4-4-12.
16. Zhou Y, Liu C.-H., Wu B. et al. Optical biopsy identification and grading of gliomas using label-free visible resonance Raman spectroscopy // Journal of Biomedical Optics. – 2019. – vol. 24. – pp. 095001 doi: 10.1117/1.JBO.24.9.095001.
17. Evans S.M., Judy K.D., Dunphy I. et al., Hypoxia Is Important in the Biology and Aggression of Human Glial Brain Tumors. // Clin Cancer Res. – 2004. – vol.10. – pp. 8177 doi: 10.1158/1078-0432.CCR-04-1081
18. Takano S., Yoshii Y., Kondo S. et al. Concentration of vascular endothelial growth factor in the serum and tumor tissue of brain tumor patients. // Cancer Res. – 1996. – vol. 56. – pp. 2185-2190.

ЛИТЕРАТУРА

1. Bailey D., Zacharia B.E. Intraoperative imaging techniques to improve tumor detection in the surgical management of gliomas // Adv. Cancer Res. – 2025. – Vol. 166. – P. 103–135. doi: 10.1016/bs.acr.2025.05.001.
2. Рында А.Ю., Олюшин Д.М., Ростовцев Д.М. и др. Результаты микрохирургической резекции глиобластом под эндоскопическим и флуоресцентным контролем // Biomedical Photonics. – 2024. – Vol. 13. – P. 20-30. doi: 10.24931/2413-9432-2024-13-3-20-30.
3. Goryaynov S.A., Okhlopkov V.A., Golbin D.A., et al. Fluorescence Diagnosis in Neurooncology: Retrospective Analysis of 653 Cases // Front. Oncol. – 2019. – Vol. 9. – P. 830. doi: 10.3389/fonc.2019.00830.
4. Потапов А.А., Горяйнов С.А., Лощенов В.Б., и др. Интраоперационная комбинированная спектроскопия (оптическая биопсия) глиом головного мозга // Журнал «Вопросы нейрохирургии» имени Н.Н. Бурденко. – 2013. – Vol. 77. – № 2. – P. 3-10.
5. Stupak E.V., Glotov V.M., Askandaryan A.S. et al. Raman Spectroscopy in the Diagnosis of Brain Gliomas: A Literature Review // Cureus. – 2025. – Vol. 17 – P. – e79165. doi: 10.7759/cureus.79165.
6. Ospanov A., Romanishkin I., Savelieva T. et al. Optical Differentiation of Brain Tumors Based on Raman Spectroscopy and Cluster Analysis Methods // Int. J. Mol. Sci. – 2023. – Vol. 24. – P. 14432. doi: 10.3390/ijms241914432.
7. Gautam, R., Vanga, S., Ariese, F. et al. Review of multidimensional data processing approaches for Raman and infrared spectroscopy // EPJ Techn Instrum. – 2015. – Vol. 2. doi: 10.1140/epjti/s40485-015-0018-6.
8. Lee J, Huh J. Pathogen Recognition via Surface-Enhanced Raman Scattering: Self-Supervised Learning and Transfer Learning approaches // ChemRxiv. – 2025. – doi: 10.26434/chemrxiv-2025-cmr8g.
9. Riva M., Sciortino T., Secoli R. et al. Glioma *biopsies* Classification Using Raman Spectroscopy and Machine Learning Models on Fresh Tissue Samples // Cancers (Basel). – 2021. – Vol. 13. – P. 1073. doi: 10.3390/cancers13051073.
10. Savelieva T., Romanishkin I., Ospanov A. et al. Machine Learning and Artificial Intelligence Systems Based on the Optical Spectral Analysis in Neuro-Oncology // Photonics. – 2025. – Vol. 12. – P. 37. doi: 10.3390/photonics12010037
11. Савельева Т.А., Романишкин И.Д., Оспанов А. и др. Методы машинного обучения для анализа спектрально-разрешенных изображений в нейроонкологии. Biomedical Photonics // 2024. – Vol. 13. – P. 40-54. doi: 10.24931/2413-9432-2024-13-4-40-54.
12. Nocera G., Sanvito F., Yao J. et al. Independent histological validation of MR-derived radio-pathomic maps of tumor cell density using image-guided biopsies in human brain tumors // J Neurooncol. – 2025. doi: 10.1007/s11060-025-05105-x.
13. Romanishkin I., Savelieva T., Kosyrkova A. et al. Differentiation of glioblastoma tissues using spontaneous Raman scattering with dimensionality reduction and data classification // Front Oncol. – 2022. – Vol. 12. – 944210. doi: 10.3389/fonc.2022.944210.
14. Романишкин И.Д., Савельева Т.А., Оспанов А. и др. Классификация внутричерепных опухолей на основе оптико-спектрального анализа // Biomedical Photonics. – 2023. – Vol. 12. – P. 4-10. doi: 10.24931/2413-9432-2023-12-3-4-10
15. Романишкин И.Д., Савельева Т.А., Оспанов А. и др. Сравнение оптико-спектральных характеристик глиобластомы при интраоперационной диагностике и оптической биопсии ex vivo // Biomedical Photonics. – 2024. – Vol. 13. – P. 4-12. doi: 10.24931/2413-9432-2024-13-4-4-12
16. Zhou Y., Liu C.-H., Wu B. et al. Optical biopsy identification and grading of gliomas using label-free visible resonance Raman spectroscopy // Journal of Biomedical Optics. – 2019. – Vol. 24. – P. 095001. doi: 10.1117/1.JBO.24.9.095001.
17. Evans S.M., Judy K.D., Dunphy I. et al., Hypoxia Is Important in the Biology and Aggression of Human Glial Brain Tumors. // Clin Cancer Res. – 2004. – Vol.10. – 8177 doi: 10.1158/1078-0432.CCR-04-1081.
18. Takano S., Yoshii Y., Kondo S. et al. Concentration of vascular endothelial growth factor in the serum and tumor tissue of brain tumor patients. // Cancer Res. – 1996. – Vol. 56. – P. 2185-2190.

19. Takahashi J.A., Fukumoto M., Igarashi K. et al. Correlation of basic fibroblast growth factor expression levels with the degree of malignancy and vascularity in human gliomas. // J Neurosurg. – 1992. – vol. 76. – pp. 792-798.
20. Scatliff J.H., Radcliffe W.B., Pittman H.H., Park C.H. Vascular structure of glioblastomas. // Am J Roentgenol Radium Ther Nucl Med. – 1969. – vol. 105. – pp. 795-805
21. Weidner N. Tumoural vascularity as a prognostic factor in cancer patients: the evidence continues to grow. // J Pathol. – 1998. – vol. 184. – pp. 119-22.
22. Brusatori M., Auner G., Noh T., et al. Intraoperative Raman Spectroscopy // Neurosurg Clin N Am. – 2017. – vol. 28. – pp. 633-652. doi: 10.1016/j.nec.2017.05.014.
23. Aydin O., Altas M., Kahraman M. et al. Differentiation of healthy brain tissue and tumors using surface enhanced Raman scattering // Appl Spectrosc. – 2009. – Vol. 63. – pp. 1095–100
24. Mehidine H., Refregiers M., Jamme F. et al. Molecular changes tracking through multiscale fluorescence microscopy differentiate Meningioma grades and non-tumoral brain tissues // Sci Rep. – 2021. – vol. 11. – pp. 3816. doi: 10.1038/s41598-020-78678-4.
25. Reichert D., Wadiura L.I., Erkkilae M.T., et al. Flavin fluorescence lifetime and autofluorescence optical redox ratio for improved visualization and classification of brain tumors // Front Oncol. – 2023. – vol. 20. – pp. 1105648. doi: 10.3389/fonc.2023.1105648.
26. Mazurek M., Szczepanek D., Orzyłowska A., Rola R. Analysis of Factors Affecting 5-ALA Fluorescence Intensity in Visualizing Glial Tumor Cells—Literature Review // International Journal of Molecular Sciences. – 2022. – vol. 23. – pp. 926. doi: 10.3390/ijms23020926.
27. Kemmner W., Wan K., Rüttinger S. et al. Silencing of human ferrochelatase causes abundant protoporphyrin-IX accumulation in colon cancer // FASEB J. – 2008. – vol. 22. – pp. 500–509.
28. Kim S., Kim J.E., Kim Y.H. et al. Glutaminase 2 expression is associated with regional heterogeneity of 5-aminolevulinic acid fluorescence in glioblastoma // Sci. Rep. – 2017. – vol. 7. – pp. 12221.
29. Utsuki S., Oka, H., Fujii K. Intraoperative Photodynamic Diagnosis of Brain Tumors Using 5-Aminolevulinic Acid // In Diagnostic Techniques and Surgical Management of Brain Tumors; Abujamra, A.L., Ed.; InTech: Rijeka, Croatia, 2011. – pp. 227–244
30. Ohgari Y., Nakayasu Y., Kitajima S. et al. Mechanisms involved in δ-aminolevulinic acid (ALA)-induced photosensitivity of tumor cells: Relation of ferrochelatase and uptake of ALA to the accumulation of protoporphyrin // Biochem. Pharmacol. – 2005. – vol. 71. – pp. 42–49.

19. Takahashi J.A., Fukumoto M., Igarashi K. et al. Correlation of basic fibroblast growth factor expression levels with the degree of malignancy and vascularity in human gliomas. // J Neurosurg. – 1992. – Vol. 76. – P. 792-798.
20. Scatliff J.H., Radcliffe W.B., Pittman H.H., Park C.H. Vascular structure of glioblastomas. // Am J Roentgenol Radium Ther Nucl Med. – 1969. – Vol. 105. – P. 795-805.
21. Weidner N. Tumoural vascularity as a prognostic factor in cancer patients: the evidence continues to grow. // J Pathol. – 1998. – Vol. 184. – P. 119-22.
22. Brusatori M., Auner G., Noh T., et al. Intraoperative Raman Spectroscopy // Neurosurg Clin N Am. – 2017. – Vol. 28. – P. 633-652. doi: 10.1016/j.nec.2017.05.014.
23. Aydin O., Altas M., Kahraman M. et al. Differentiation of healthy brain tissue and tumors using surface enhanced Raman scattering // Appl Spectrosc. – 2009. –Vol. 63. – P. 1095–100.
24. Mehidine H., Refregiers M., Jamme F. et al. Molecular changes tracking through multiscale fluorescence microscopy differentiate Meningioma grades and non-tumoral brain tissues // Sci Rep. – 2021. – Vol. 11. – P. 381. doi: 10.1038/s41598-020-78678-4.
25. Reichert D., Wadiura L.I., Erkkilae M.T., et al. Flavin fluorescence lifetime and autofluorescence optical redox ratio for improved visualization and classification of brain tumors // Front Oncol. – 2023. – Vol. 20. – P. 1105648. doi: 10.3389/fonc.2023.1105648.
26. Mazurek M., Szczepanek D., Orzyłowska A., Rola R. Analysis of Factors Affecting 5-ALA Fluorescence Intensity in Visualizing Glial Tumor Cells—Literature Review // International Journal of Molecular Sciences. – 2022. – Vol. 23. – P. 926. doi: 10.3390/ijms23020926
27. Kemmner W., Wan K., Rüttinger S. et al. Silencing of human ferrochelatase causes abundant protoporphyrin-IX accumulation in colon cancer // FASEB J. – 2008. – Vol. 22. – P. 500–509,
28. Kim S., Kim J.E., Kim Y.H. et al. Glutaminase 2 expression is associated with regional heterogeneity of 5-aminolevulinic acid fluorescence in glioblastoma // Sci. Rep. – 2017. – Vol. 7. – P. 12221.
29. Utsuki S., Oka, H., Fujii K. Intraoperative Photodynamic Diagnosis of Brain Tumors Using 5-Aminolevulinic Acid // In Diagnostic Techniques and Surgical Management of Brain Tumors; Abujamra, A.L., Ed.; InTech: Rijeka, Croatia, 2011. – P. 227–244
30. Ohgari Y., Nakayasu Y., Kitajima S. et al. Mechanisms involved in δ-aminolevulinic acid (ALA)-induced photosensitivity of tumor cells: Relation of ferrochelatase and uptake of ALA to the accumulation of protoporphyrin // Biochem. Pharmacol. – 2005. – Vol. 71. – P. 42–49.